DIRECT NUMERICAL SIMULATION OF TURBULENT OPEN CHANNEL FLOW WITH FROUDE NUMBER EFFECT

Jin Lee, Jungsoo Suh and Hyung Jin Sung*
Department of Mechanical Engineering, KAIST
291 Daehak-ro, Yuseong-gu, Daejeon, 305-701, Korea
Lee.Jin@kaist.ac.kr, jssuh@khnp.co.kr, hjsung@kaist.ac.kr

ABSTRACT

Direct numerical simulation (DNS) of open-channel flow in the presence of an air-water interface was performed to examine the effects of interface deformation on the turbulence structures. In the water-driven turbulence, flows characterized by either of two Froude numbers (Fr=0.2 and 0.8) were examined and compared. A coupled level-set and volume-of-fluid (CLSVOF) method was employed to track the interface. The air that contacted the water was entrained into the turbulent flow. At high Fr, all turbulent normal stresses on the air side of the interface were high near the sidewall. Moreover, all terms of the Reynolds shear stress were intensified at the mixed-boundary corner on the air side of the interface. Two-point correlations between the streamwise vortex and the velocity fluctuations provided structural information about the near-wall streaky structures and the inner secondary flows in the cross-stream plane. Linear stochastic estimates of the conditionally averaged flow field showed that the inner secondary flow consisted of not only in-plane velocity components but also streamwise velocity components.

INTRODUCTION

The modeling of turbulent open-channel flows near sidewalls has been an important topic in fluid dynamics because the physics of such flows may be applied practically in fluid and ocean engineering. Flows around ship hulls and marine structures are the most common examples of such flow geometries. In nature, the flow of rivers may be described using this framework. A crucial feature of such flows is the interaction between the wall turbulence and the air-water interface (Broglia *et al*., 2003). Unlike open-channel flows without sidewalls, open-channel flows with sidewalls involve mixed-boundary corner flows that occur at the junctures of a solid wall and an air-water interface. The presence of a sidewall induces highly anisotropic and physically complex flows in turbulent coherent structures. Because organized motions play crucial roles in the production and dissipation of wall turbulence (Robinson, 1991), understanding the coherent structures and turbulence statistics in such flows is essential to an understanding of mixed-boundary corner flow structures.

Few numerical investigations have addressed open-channel flows with both sidewalls and air-water interfaces. Shi *et al*. (1999) conducted large-eddy simulations (LESs) of open-channel flows and showed that the datasets obtained from simulation agreed well with the experimental data. Broglia *et al*. (2003) studied systems with Re_τ=360, 600 and 1000 using LESs. They observed that flow in the mixed-boundary corner was significantly influenced by advection due to the inner and outer secondary flows. A budget analysis of the Reynolds stress showed that both production and dissipation terms decreased toward the free surface. Joung and Choi (2010) performed DNSs and showed that the production of Reynolds shear stress and secondary flows was determined by the directional tendencies of the dominant coherent structures. However, their studies examined a forced flat interface. Several open issues must be resolved to elucidate the effects of the deformable air-water interface on turbulence statistics and coherent structures.

The main objective of the present study was to gain insight into the dynamics of the mixed-boundary corner by examining the turbulence statistics and the coherent structures. We carried out DNSs of the turbulence open-channel flows to elucidate the effects of the deformation of the air-water interface. To investigate the effects, simulations were conducted at three Froude numbers Fr=0.2, 0.5, and 0.8. The Reynolds number was fixed at Re=5,600 to reflect the bulk mean velocity. A schematic diagram of the computational domain is shown in Figure 1. The effects of the deformable interface on the mixed-boundary corner were investigated by examining the mean flow, the Reynolds stresses, and the budget of the turbulent kinetic energy. Finally, two-point correlations and linear stochastic estimations of conditionally averaged fields were used to determine the statistical properties of individual streamwise vortices with velocity fluctuations.

NUMERICAL METHOD

In the present work, the coupled level-set and volume-of-fluid (CLSVOF) method was selected among the many numerical methods available for interface modeling. In the CLSVOF method, the level-set (LS) function ϕ is defined as the distance function from the interface and is positive in the liquid, negative in the gas, and zero at the interface. The volume-of-fluid (VOF) function F is defined as the liquid volume fraction in each cell. In the present work, the interface was captured using a VOF function with the aid of an LS function for calculating the vector normal to the interface. The

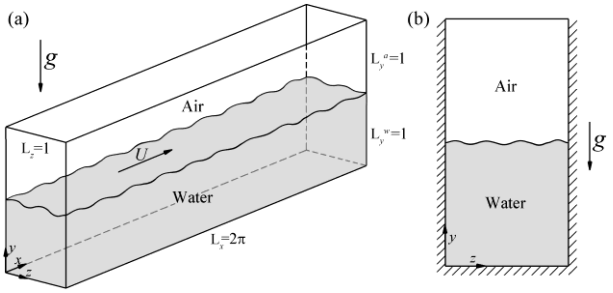

Figure 1. Schematic diagram of the computational domain and coordinate system; (a) 3-D view and (b) cross-stream planar view

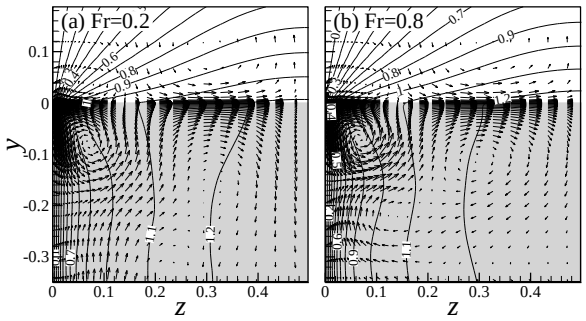

Figure 2. Mean streamwise velocity contours and secondary velocity vectors. (a) Fr=0.2 and (b) Fr=0.8.

VOF and LS functions were advanced in time using following equations, respectively,

$$\frac{\mathrm{D}F}{\mathrm{D}t} = \frac{\partial F}{\partial t} + (\mathbf{u}\cdot\nabla)F = 0\,, \tag{1}$$

$$\frac{\mathrm{D}\phi}{\mathrm{D}t} = \frac{\partial \phi}{\partial t} + (\mathbf{u}\cdot\nabla)\phi = 0\,. \tag{2}$$

The governing equations describing the incompressible viscous flow of two immiscible fluids are

$$\frac{\partial \mathbf{u}}{\partial t} + \mathbf{u}\cdot\nabla\mathbf{u} = \frac{1}{\rho}\nabla\cdot(-p\mathbf{I}+\mathbf{T}) + \mathbf{g}\,, \tag{3}$$

$$\nabla\cdot\mathbf{u} = 0\,, \tag{4}$$

where t is time, $\mathbf{u}$ is the velocity vector, p is the pressure, $\mathbf{I}$ is the unit tensor, ρ is the density, $\mathbf{g}$ represents the gravity, and $\mathbf{T}$ is the viscous stress tensor defined as $\mathbf{T}=2\mu\mathbf{S}$. Here, μ is the dynamic viscosity, $\mathbf{S}$ the strain rate tensor given by

$$\mathbf{S} = \frac{1}{2}\left[\nabla\mathbf{u} + (\nabla\mathbf{u})^{\mathrm{T}}\right], \tag{5}$$

where the superscript T represents the transpose operation. The governing equations were integrated in time using the fractional step method. The Navier-Stokes equation solver, which was originally based on the implicit velocity decoupling procedure proposed by Kim *et al*. (2002), was modified to yield a second-order semi-implicit scheme. In this approach, the diagonal viscous terms were discretized using the Crank-Nicolson method, and the convective terms and other viscous terms were discretized using the second-order Adams-Bashforth scheme. All terms were resolved using a second-order central difference scheme in space with a staggered mesh.

Coordinates were chosen such that x, y, and z corresponded to the streamwise, vertical, and spanwise directions, respectively (see Figure 1). The domain size used in the present DNS was $2\pi L\times 2L\times L$ in the x-, y-, and z-directions, respectively. The grid spacing was uniform in the streamwise direction and the grid points in the wall-normal and the spanwise directions were clustered near the solid wall and the air-water interface according to a hyperbolic tangent distribution. A no-slip condition was imposed at the side walls and bottom wall. Periodic boundary conditions were applied along the streamwise direction. Note that two cases (Fr=0.2, mild, and 0.8, strong) are considered in depth in the following discussion, although three cases (Fr=0.2, 0.5 and 0.8) were modeled in the present study. The effects of interfacial deformations were tested holding the Reynolds number constant (Re=5,600), consistent with the bulk mean velocity for the three cases. The reliability and accuracy of the present numerical simulations were ascertained by comparing the turbulence statistics with measures of the experimental and numerical data. The mean velocity and turbulence intensities along the wall bisector agreed well with those of previous results (Nezu and Rodi, 1986; Broglia *et al*., 2003; Joung and Choi, 2010).

TURBULENCE STATISTICS

Mean Properties

Turbulence statistics at a mixed-boundary corner formed by a solid wall and an air-water interface were examined. Figure 2 shows the mean streamwise velocity contours with cross-stream velocity vectors, and all velocity components were normalized by the bulk streamwise velocity. As Fr increased, the high-speed mean streamwise velocity increased beneath the interface, which decreased the interface elevation. Due to the presence of the air-water interface, asymmetric counter-rotating vortices formed, which consisted of inner and outer mean secondary flows. These are known to play important roles in momentum transport near the boundary between the air-water interface and vertical no-slip walls. The inner secondary flows transfer high-momentum fluids from the air-water interface toward the sidewall. This result contributed negligibly to the interfacial deformation and the strength of the mean streamwise vortices. As Fr decreased, the location of the core of the outer secondary flows moved deeper toward the bottom of the wall. The location of the core of the inner secondary flow was unrelated to Fr, and the core was located 0.06 from both the sidewall and the air-water interface. Moreover, upward motion near the sidewall ($z\approx 0$) and downward motion near the bottom-wall bisector ($z\approx 0.5$) agreed with the results of a previous study of open-channel turbulent flow. The time-averaged vertical motion inside the water was vigorous when the air-water interface was less deformable.

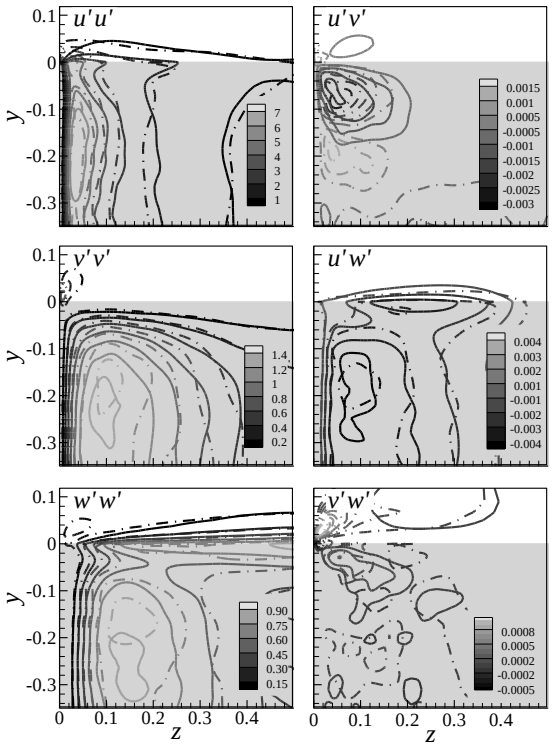

Figure 3. Reynolds stress distributions normalized by the friction velocity. Solid line and dash-dot line represent Fr=0.2 and Fr=0.8, respectively.

Figure 2 also shows the mean streamwise velocities on the air side. The spanwise motion at the interface flowed in the same direction as the water, and the vertical motion proceeded away from the water near the air-water interface. As a result, the fluid (initially at rest) and the air produced a pair of counter-rotating vortices in the cross-stream plane. The downward motion of the air was observed between z=0.1 and z=0.2 in the cross-stream plane. This indicated that the air in contact with the water was entrained with the turbulent flow and experienced velocity fluctuations due to the turbulent flow of the water. However, the Froude number did not significantly affect the strength of the time-averaged air flow, which was mainly sensitive to the streamwise velocity of the water rather than the elevation of the air-water interface.

Second-order Turbulence Statistics

The Fr number significantly affected the second-order statistics near the air-water interface. The distributions of the normal velocity fluctuations in the cross-stream plane are shown in Figure 3, which shows the contours normalized by the friction velocity. The flow patterns modeled by the DNS were qualitatively consistent with those predicted by simulations involving the flat air-water interface. Because the distributions of all normal stress components in regions away from the air-water interface were similar to those under the flat air-water interface conditions, the flows near the mixed-boundary corner were found to be focused. On the air side, the spatial extent of the contours for the streamwise normal stress *u'u'* increased near the sidewall at high Fr, whereas the spatial extent of the contours on the water side were consistent, regardless of Fr. On the other hand, the gradient of the vertical velocity fluctuations indicated the thickness of the blockage layer beyond which the kinematic boundary conditions were affected (Shen *et al*., 1999). As shown in Figure 3, the vertical gradient of the vertical normal stress decreased near the interface with the bottom-wall bisector, i.e., the thickness of the blockage layer became thinner as Fr increased. At the mixed-boundary corner on the air side, the vertical normal stress was finite only for Fr=0.8, where the splats (fluid moving toward the air-water interface) were frequently observed. The spanwise normal stress *w'w'* above the interface increased, whereas that beneath the interface decreased as Fr increased.

Figure 3 also shows the spatial distributions of the Reynolds shear stresses normalized by the friction velocity. At high applied Fr, all terms of the Reynolds shear stress were intensified at the mixed-boundary corner on the air side. Complex deformations at the wavy interface due to high Fr conditions complicated the flow fields near the mixed-boundary corner. Under high Fr conditions, positive values of *u'v'* were created beneath the inner secondary flow but were not observed in the flat air-water interface simulations. Because positive *u'v'* resulted from the upward sweeps and downward ejections (Joung and Choi, 2010), the clockwise rotation of vortices was expected to dominate the inner secondary flow at higher Fr. Near the interface, the spatial extent of the negative values of *u'w'* was reduced for Fr=0.8 because the vertical velocity fluctuations near the interface did not significantly convert into the interface-parallel velocities in the reduced thickness of the blockage layer. The contours of the cross-plane shear stress *v'w'* exhibited rather poor convergence, although many statistical samples were used. The extents under high Fr conditions were smaller than those for lower Fr near the mixed-boundary corner, but they had finite values beneath the corner.

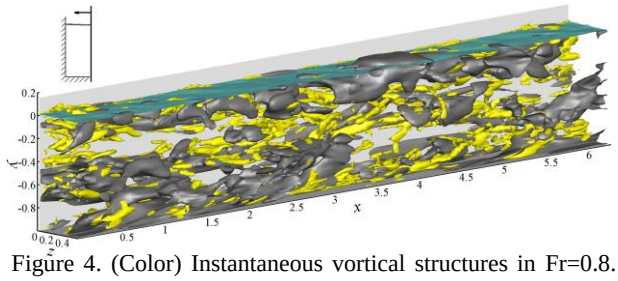

Figure 4. (Color) Instantaneous vortical structures in Fr=0.8. The vortical structures are shown as yellow isosurface plots of the swirling strength (10% of the maximum λ_{ci}). The black area indicates the low-speed regions (10% below the bulk mean velocity).

TURBULENT COHERENT STRUCTURES

In this section, we focus on the interfacial deformation and its effects on the formation of streaky structures and vortical structures by examining the instantaneous flow fields and their statistical properties. In the present study, the turbulent swirling strength λ_{ci} was employed to distinguish the vortical structures from the background turbulence. Unlike the vorticity, the swirling strength did not show regions of intense shear, but effectively identified the true vortex cores. Half volumes of the 3D flow fields of the swirling strength and the low-speed streaks in Fr=0.8 are shown in Figure 4. Several elongated low-speed regions were present, and each lay enclosed by the vortical structures. The location of the vortical structure in the air side was consistent with the position of the wavy air-water interface. The vortical structures connected to the interface provided an energy transport mechanism from the surface to each fluid (Grega *et al*., 1995). The flow structures of the three Froude numbers were qualitatively similar except for the strength of the vortical structures on the surface, which originated from the surface elevation.

Near-wall Streaky Structures

Several types of structures were identified in the wall turbulence: low-speed streaks, high-speed streaks, and quasi-streamwise vortices were the dominant coherent structures in the near-wall region. These structures were closely related to the production of wall turbulence (Robinson, 1991). Because wall turbulence varied with the geometry and was sensitive to the presence of an air-water interface and sidewalls, our discussion focused on the variations of the near-sidewall streaky structures and the statistical properties due to the presence of an air-water interface and Fr effects. The instantaneous characteristics of streamwise velocity streaks in the *xy* plane at $z^+\approx5.5$ for Fr=0.2 and 0.8 systems (not shown) were qualitatively similar except near the air-water interface ($y\approx0$). In this region, the streaks in Fr=0.8 were shorter and stronger than those in Fr=0.2. The low-speed streaks were longer and narrower than the high-speed streaks in both flows. In addition, high-speed streaks were more commonly observed than low-speed streaks in the vicinity of the air-water interface. Because instantaneous distributions cannot quantitatively define the structural information without ambiguity, a statistical analysis was necessary. To quantify the spatial coherence and understand the statistical significance of various features within the velocity fields, two-point correlations of the fluctuating velocity components were calculated. The two-point correlations between any two quantities R_{AB} are defined as

$$R_{AB}(r_x, y_{ref}, z_{ref}) = \frac{\langle A(x, y_{ref}, z_{ref}) B(x + r_x, y_{ref}, z_{ref}) \rangle}{\sigma_A(y_{ref}, z_{ref}) \sigma_B(y, z)}, \quad (6)$$

where y_{ref} and z_{ref} are the reference vertical and spanwise positions at which the correlation is computed. σ_A (y_{ref}, z_{ref}) and σ_B (y, z) are the root-mean-squares of A and B, respectively, and r_x is the in-plane streamwise separation between A and B. The two-point correlations between the streamwise velocity fluctuations R_{uu} at $z^+\approx5.5$ in the sidewall-parallel plane are shown in Figure 5. The average streamwise dimension of the correlations in the Fr=0.8 system was shorter than that in the Fr=0.2 system for a reference position of $y^+_{ref}=0$. In contrast with previous observations of the flat air-water interface (Grega et al., 1995), the surface deformations disturbed the evolution of large-scale streaky structures. However, the streamwise dimensions of $y^+_{ref}=-19.2$ increased as Fr increased. This result showed that the most frequent positions of the streaky structures near the interface were shifted away from the air-water interface. The streamwise dimensions of the correlations further below the surface ($y^+_{ref}=-38.5$) were more similar because the influences of the surface deformations were smaller.

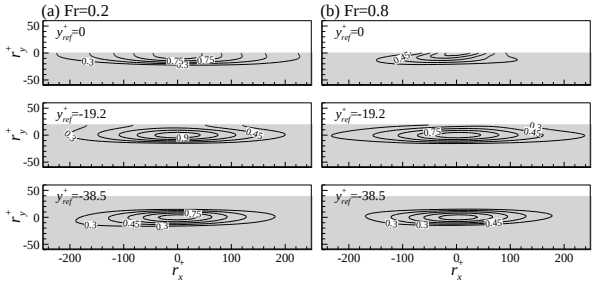

Figure 5. Two-point correlations of the streamwise velocity fluctuations at $z^+=5.5$. Contour levels are from 0.3 to 0.9 with increments of 0.15. (a) Fr=0.2 and (b) Fr=0.8.

Statistical Properties of Streamwise Swirl

Previous numerical and experimental studies of open-channel flows have shown that the inner secondary flow and its transport are important types of organized structures on mixed-boundary corners (Grega *et al*., 1995; Hsu *et al*., 2000). These structures are closely related to turbulent energy transport mechanisms in the mixed-boundary corner. Two-point correlations between streamwise vortices and velocity fluctuations were calculated to obtain structural information about the inner secondary flows in the cross-stream plane. These correlations are useful for estimating the conditionally averaged velocity fields for a given vortex core and show the average velocity fields associated with a vortex core located at a reference point. In this section, the streamwise vortical structures were identified via the swirling-strength parameter $\Lambda_{ci,x}$, which is a signed swirling strength calculated from the 2-D velocity gradient tensor in the cross-stream plane ($\underline{\underline{D}}^{2\text{-}D}_{yz}$).

Figures 6(a)-(b) show the contours of the two-point correlations between the swirling strength parameter and the wall-normal velocity fluctuations $R_{\Lambda v}$ at the core of the inner secondary flows. The statistically dominant fluid motions around the vortex core could be determined from the correlations. Because the core rotated in the counter-clockwise direction, $R_{\Lambda v}$ was positive on the right-hand side and negative on the left-hand side of the reference position. Positive

contours beneath the interface contacted the negative contours above the interface. The fluid motion induced by the coherent structures interacted with the fluid flowing in the opposite direction via the deformable interface. The spatial extents of the correlations above the interface decreased slightly with increasing Fr, whereas the spatial extents beneath the interface were similar for all Fr. The correlations between the swirling strength parameter and the spanwise velocity fluctuations $R_{\Lambda w}$ are shown in Figures. 6(c)-(d). The positive and negative $R_{\Lambda w}$ were predominant below the core and above the reference point, respectively. The spatial extent of $R_{\Lambda w}$ decreased with increasing Fr. This result showed that the streamwise vortices statistically induced fluid motions in both systems, and their correlations at the contacted fluid decreased slightly at high Fr. The inner secondary flow induced interfacial deformation, and the vortical structure on the deformable interface caused motion on the air side, as shown in Figure 4. However, Fr did not affect the strength of the inner secondary flow or its reflected motion at the air side. Thus, the velocity vectors on the air side were determined by complex physics involving the strength of the inner secondary flow and the interfacial deformation.

Linear stochastic estimation (LSE) methods were employed to obtain quantitative structural information about the streamwise-oriented swirling event. LSE is a robust conditionally averaged approximation that provides satisfactory results for various turbulent fields. The linear

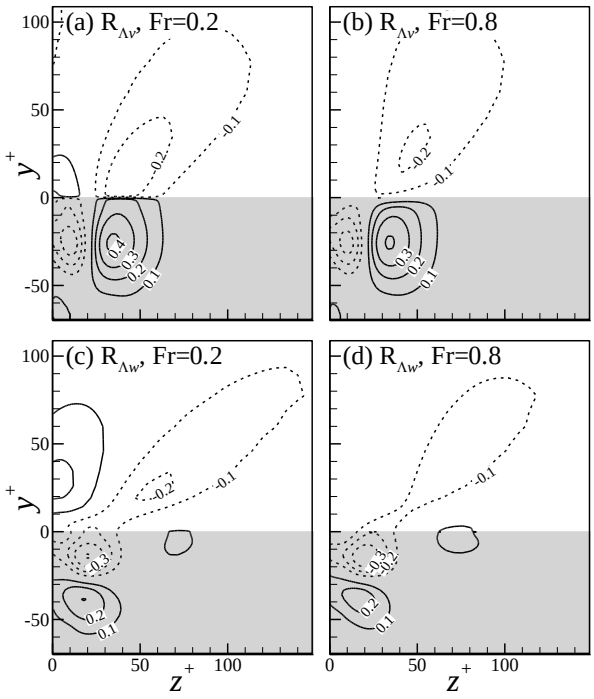

Figure 6. Two-point correlations between (a)-(b) the positive swirling strength parameter and the vertical velocity, and between (c)-(d) the positive swirling strength parameter and the spanwise velocity at y^+=-26 and z^+=24.

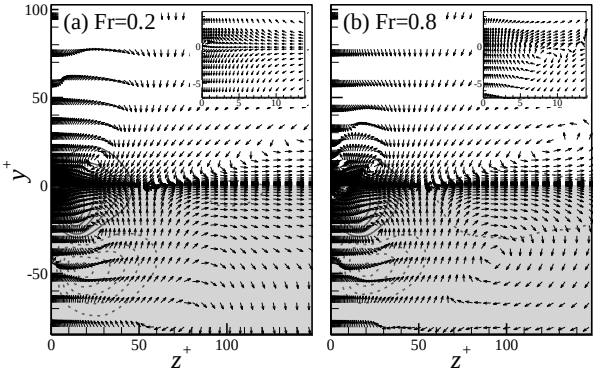

Figure 7. Linear estimate of the conditionally averaged velocity field based on the positive swirling-strength parameter at y^+=-26 and z^+=24. Contours are shown in the background to indicate the streamwise velocity normalized by the friction velocity. (a) Fr=0.2 and (b) Fr=0.8.

estimate of the conditional average is given by

$$\left\langle u_i(x+r) \mid \Lambda_{ci,x}(x) \right\rangle \approx L_i \Lambda_{ci,x}(x), \qquad (7)$$

where the kernel L_i is determined by minimizing the mean-square error between the estimate and the conditional average, and is given as

$$L_i = \frac{\left\langle u_i(x+r)\Lambda_{ci,x}(x) \right\rangle}{\left\langle \Lambda_{ci,x}(x)^2 \right\rangle}. \qquad (8)$$

The flow structures for Fr=0.2 and Fr=0.8 systems are shown in Figure 7, and the estimations associated with the positive swirling-strength parameters correspond to the cores of the inner secondary flows. The velocity vector was uniformized, and the vector grid spacing was down-sampled for clarity. The streamwise vortex structures were visible not only at the event position corresponding to the inner secondary flow but also at the position of the outer secondary flow. Considerable coherence between the vortices was ascertained using conditional averaging, although coherence was only observed in the time-averaged properties. This result revealed a downward motion of the air, which represented the coherence of the inner secondary flow and the fluid entrained toward the interface. Because the location of the downward motion occurred at positions near the interface that corresponded to the positions of splats from the counter-rotating streamwise vortex pair, this result implied that the interaction between the inner and outer secondary flow dominated entrainment of the opposite fluid. Furthermore, the positive and negative streamwise velocity fluctuations were predominant below and above the reference point, respectively. The inner secondary flow consisted of not only the in-plane velocity components, but also the streamwise velocity, suggesting that the flow regime was fully three-dimensional. The counter-clockwise streamwise vortex was located on the right-hand side of the positive streamwise velocity and on the left-hand side of the negative streamwise velocity (Lee *et al.*,

2010). Because the vortex corresponded to the inner secondary flow, the secondary flow was considered as a leg of a hairpin-like vortex in the wall turbulence.

Under high Fr conditions (Fr=0.8), an additional streamwise vortex was found at the mixed-boundary corner, and this vortex rotated the same direction as the outer secondary flow (see the box in Figure 7(b)). Although the strength of the vector was quite weak, it confined the range in which antisplats occurred. Moreover, the spatial extent and strength of the streamwise velocity decreased near the corner as Fr increased. The vertical position of the core of the outer secondary flow under low Fr conditions was deeper than that under high Fr conditions. However, the spanwise distance from the core of the inner and outer secondary flow was smaller in the low Fr flow. The overall spacing between the cores was quite similar, although the vertical and spanwise distance was altered. These observations are consistent with the mean cross-stream velocity vectors, as shown in Figure 2.

CONCLUSIONS

A DNS of an open-channel flow with an air-water interface was performed to elucidate the effects of deformation of the air-water interface on its turbulence statistics and coherent structures at a mixed-boundary corner. In this water-driven flow, two Froude number flow conditions (Fr=0.2 and 0.8) were examined for comparison. The coupled level-set and volume-of-fluid (CLSVOF) method was employed to track the interface. The mean streamwise velocity contours revealed that the inner and outer secondary flows were observed in the present DNS. Under high Fr conditions, the position of the outer secondary flow core moved deeper toward the bottom wall, whereas the inner flow core position remained unchanged. In the present two-phase fluid flow, the air that contacted the water was entrained in the turbulent flow. Under high Fr conditions, all turbulent normal stresses on the air side increased near the sidewall, where the interface elevation varied vigorously. The thickness of the blockage layer thinned as Fr increased. Moreover, all terms of the Reynolds shear stress were intensified at the mixed-boundary corner on the air side. The turbulent coherent structures were statistically analyzed to provide a comprehensive analysis of the nature of the open-channel flow. The coherent velocity structures near the sidewall were shorter in the vicinity of the air-water interface due to the deformable interface. The two-point correlations between the streamwise vortex and the velocity fluctuations were calculated to obtain structural information about the inner secondary flows in the cross-stream plane. Finally, structural information about the inner secondary flow in the cross-stream plane was obtained by examining the correlations and the linear stochastic estimations of the conditionally averaged flow field. The spatial extent of the correlation $R_{\Lambda v}$ above the interface decreased with increasing Fr, whereas that beneath the interface was relatively insensitive to Fr. The spatial extent of the correlation $R_{\Lambda w}$ decreased with increasing Fr. The inner secondary flow consisted not only of in-plane velocity components, but also of streamwise velocity components, which corresponded to a leg of the hairpin-like vortex. An additional streamwise vortex was observed at the mixed-boundary corner in flows with a highly deformable interface.

ACKNOWLEDGEMENT

This work was supported by the Creative Research Initiatives (No. 2011-0000423) of the National Research Foundation of Korea.

REFERENCES

Broglia, R., Pascarelli, A., and Piomelli, U., 2003, "Large-eddy simulations of ducts with a free surface", *Journal of Fluid Mechanics*, Vol. 484, pp. 223-253.

Grega, L. M., Wei, T., Leighton, R. I., and Neves, J. C., 1995, "Turbulent mixed-boundary flow in a corner formed by a solid wall and a free surface", *Journal of Fluid Mechanics*, Vol. 294, pp. 17-46.

Hsu, T. Y., Grega, L. M., Leighton, R. I., and Wei, T., 2000, "Turbulent kinetic energy transport in a corner formed by a solid wall and a free surface", *Journal of Fluid Mechanics*, Vol. 410, 343-366.

Joung, Y. and Choi, S.-U., 2009, "Direct numerical simulation of low Reynolds number flows in an open-channel with sidewalls", *International Journal for Numerical Methods in Fluids*, Vol. 62, pp. 854-874.

Kim, K., Baek, S.-J., and Sung, H. J., 2002, "An implicit decoupling procedure for the incompressible Navier-Stokes equations", *International Journal for Numerical Methods in Fluids*, Vol. 38, pp. 125-138.

Nezu, I., and Rodi, W., 1986, "Open-channel flow measurements with a Laser Doppler anemometer", *Journal of Hydraulic Engineering-ASCE*, Vol. 112, pp. 335-355.

Robinson, S. K., 1991, "Coherent motions in the turbulent boundary layer", *Annual Review of Fluid Mechanics*, Vol. 23, pp. 601-639.

Shen, L., Zhang, X., Yue, D. K. P., Triantafyllou, and G. S., 1999, "The surface layer for free-surface turbulent flows", *Journal of Fluid Mechanics*, Vol. 386, pp. 167-212.

Shi, J., Thomas, T. G., and Williams, J. J. R., 1999, "Large-eddy simulation in a rectangular open channel", *Journal of Hydraulic Research*, Vol. 37, pp. 345-361.

Wang, Z., Yang, J., Koo, B., and Stern, F., 2009, "A coupled level set and volume-of-fluid method for sharp interface simulation of plunging breaking waves", *International Journal of Multiphase Flow*, Vol. 35, pp. 227–246.